Reviewing Global Estimates of Surface Reactive Nitrogen Concentration and Deposition Using Satellite Retrievals

Lei Liu [a, *], Xiuying Zhang [b], Wen Xu [c], Xuejun Liu [c], Xuehe Lu [b], Jing Wei [d, e], Yi Li [f], Yuyu Yang [a], Zhen Wang [b], Anthony Y. H. Wong [g]

[a] College of Earth and Environmental Sciences, Lanzhou University, Lanzhou 730000, China

[b] International Institute for Earth System Science, Nanjing University, Nanjing, 210023, China

[c] College of Resources and Environmental Sciences, National Academy of Agriculture Green Development, China Agricultural University, Beijing, 100193, China

[d] State Key Laboratory of Remote Sensing Science, College of Global Change and Earth System Science, Beijing Normal University, Beijing, China

[e] Department of Atmospheric and Oceanic Science, Earth System Science Interdisciplinary Center, University of Maryland, College Park, MD, USA

[f] Chief Technology Officer SailBri Cooper Inc., Beaverton OR, 97008, USA

[g] Department of Earth and Environment, Boston University, Boston, MA 02215, USA

* Correspondence to Lei Liu (liuleigeo@lzu.edu.cn).

Abstract

Since the industrial revolution, human activities have dramatically changed the nitrogen (N) cycle in natural systems. Anthropogenic emissions of reactive nitrogen (N_r) can return to the earth's surface through atmospheric N_r deposition. Increased N_r deposition may improve ecosystem productivity. However, excessive N_r deposition can cause a series of negative effects on ecosystem health, biodiversity, soil, and water. Thus, accurate estimations of N_r deposition are necessary for evaluating its

environmental impacts. The United States, Canada and Europe have successively launched a number of satellites with sensors that allow retrieval of atmospheric NO_2 and NH_3 column density, and therefore estimation of surface N_r concentration and deposition at an unprecedented spatiotemporal scale. Atmosphere NH_3 column can be retrieved from atmospheric infra-red emission, while atmospheric NO_2 column can be retrieved from reflected solar radiation. In recent years, scientists attempted to estimate surface N_r concentration and deposition using satellite retrieval of atmospheric NO_2 and NH_3 columns. In this study, we give a thorough review on recent advances of estimating surface N_r concentration and deposition using the satellite retrievals of NO_2 and NH_3, present a framework of using satellite data to estimate surface N_r concentration and deposition based on recent works, and summarize the existing challenges for estimating surface N_r concentration and deposition using the satellite-based methods. We believe that exploiting satellite data to estimate N_r deposition has a broad and promising prospect.

Keywords

Nitrogen deposition; Satellite retrieval; Surface concentration; Oxidized and reduced N_r

1. Introduction

Nitrogen (N) exists in three forms in the environment including reactive nitrogen (N_r), organic nitrogen (ON) and nitrogen gas (N_2) (Canfield et al., 2010). N_2 is the main component of air, accounting for 78% of the total volume of air, but it cannot be directly used by most plants. N_r refers to the general term of N-containing substances in atmosphere, plants, soils and fertilizers that are not combined with carbon. N_r (such as NO_3^- and NH_4^+) is the main form of N that can be directly used by most plants, but the content of N_r in nature is much lower compared with ON and N_2 (Vitousek et al.,

1997;Nicolas and Galloway, 2008). The supply of N_r is essential for all life forms and contributes to the increase in agricultural production, thus providing sufficient food for the growing global population (Galloway et al., 2008;David et al., 2013;Galloway et al., 2004b;Erisman et al., 2008). Before the industrial revolution, N_r mainly came from natural sources such as biological N fixation, lightning and volcanic eruption (Galloway et al., 2004a). Since the industrial revolution, human activities (e.g. agricultural development, combustion of fossil energy) have greatly perturbed the N cycle in natural systems (Canfield et al., 2010;Kim et al., 2014;Lamarque et al., 2005).

N_r (NO_x and NH_3) emitted to the atmosphere will return to the earth surface through atmospheric deposition (Liu et al., 2011). Atmospheric N_r deposition refers to the process in which N_r are removed from the atmosphere, including wet (rain and snow) and dry (gravitational settling, atmospheric turbulence, etc.) deposition (Xu et al., 2015;Zhang et al., 2012;Pan et al., 2012). The input of N_r over terrestrial natural ecosystems primarily comes from the N_r deposition (Shen et al., 2013;Sutton et al., 2001;Larssen et al., 2011). In the short term, atmospheric N_r deposition can increase the N_r input to ecosystems, which promotes plant growth and enhances ecosystem productivity (Erisman et al., 2008;Sutton et al., 2013). However, excessive atmospheric N_r deposition also causes a series of environmental problems (Liu et al., 2017d). Due to the low efficiency of agricultural N application, plenty of N_r is lost through runoff, leaching and volatilization, causing serious environmental pollution. Excessive N_r deposition may aggravate the plant's susceptibility to drought or frost, reduce the resistance of plant to pathogens or pests, and further affect the physiology and biomass distribution of vegetation (ratio of roots, stems and leaves) (Stevens et al., 2004;Nadelhoffer et al., 1999;Bobbink et al., 2010;Janssens et al., 2010). Excessive

N_r leads to eutrophication and related algal blooms over aquatic ecosystems, reducing water biodiversity (Paerl et al., 2014), while excessive N_r in drinking water also poses a threat to human health (Zhao et al., 2013). Therefore, monitoring and estimation of surface N_r concentration and deposition on the global scale are of great importance and urgency.

The methods of estimating atmospheric N_r deposition can be divided into three categories: ground-based monitoring, atmospheric chemical transport modeling (ACTM) and satellite-based estimation. Ground-based monitoring is considered to be the most accurate and quantitative method, which can effectively reflect the N_r deposition in local areas. ACTM can simulate the processes of N_r chemical reaction, transport, and deposition, as well as the vertical distribution of N_r. Satellite-based estimation establishes empirical, physical or semi-empirical models by connecting the ground-based N_r concentrations and deposition with satellite-derived N_r concentration. This study focuses on reviewing the recent development of satellite-based methods to estimate N_r deposition. Since the estimation of N_r concentrations is just a part of the estimation of dry N_r depositions, we here mainly reviewed the progress of dry N_r depositions using the satellite observation. We firstly give a brief introduction to the progress of ground-based monitoring, ACTM-based methods, and then present a detailed framework of using satellite observation to estimate dry and wet N_r deposition (including both oxidized and reduced N_r). Next, we review the recent advances of the satellite-based methods of estimating N_r deposition. Finally, we discuss the remaining challenges for estimating surface N_r concentration and deposition using satellite observation.

2 Methods for Estimating Surface N_r Concentration and Deposition

2.1 Ground-based Monitoring

Ground-based monitoring of N_r deposition can be divided into two parts: wet and dry N_r deposition monitoring. Since the 1970s, there have been large-scale monitoring networks focusing on the wet N_r deposition. The main large-scale regional monitoring networks include Canadian Air and Precipitation Monitoring Network (CAPMoN), Acid Deposition Monitoring Network in East Asia (EANET), European Monitoring and Evaluation Program (EMEP), United States National Atmospheric Deposition Program (NADP), World Meteorological Organization Global Atmosphere Watch Precipitation Chemistry Program, and Nationwide Nitrogen Deposition Monitoring Network in China (NNDMN) (Tan et al., 2018;Vet et al., 2014). The detailed scientific objectives of the wet N_r deposition observation networks vary, but most of the observation networks mainly concentrate on the spatiotemporal variation of wet deposition of ions including N_r compounds, the long-term trends of ions in precipitation, and the evaluation of ACTMs.

Compared with wet N_r deposition monitoring, dry N_r deposition monitoring started late, due to the limitation of monitoring technology since it is more difficult to be quantified (affected greatly by surface roughness, air humidity, climate and other environmental factors) (Liu et al., 2017c). Dry N_r deposition observation networks include US ammonia monitoring network (AMoN), CAPMoN, EANET and EMEP. The monitoring methods of dry N_r deposition are mainly divided into direct monitoring (such as dynamic chambers) and indirect monitoring (such as inferential methods). The inferential model is widely applied in ground-based monitoring networks (such as EANET and NNDMN), mainly because this method is more practical and simpler. In inferential models, dry deposition is divided into two parts:

surface N_r concentrations and the deposition velocity (V_d) of N_r (Nowlan et al., 2014). V_d can be estimated by meteorology, land use types of underlying surface as well as the characteristics of each N_r component itself using resistance models (Nemitz et al., 2001). Thus, dry N_r deposition monitoring networks only need to focus on the quantification of surface concentration of individual N_r components. The N_r components in the atmosphere are very complex, including N_2O_5, HONO, NH_3, NO_2, HNO_3 and particulate NH_4^+ and NO_3^-. Most monitoring networks include the major N_r species such as gaseous NH_3, NO_2, HNO_3 and the particles of NH_4^+ and NO_3^-.

Effort of ground-based N_r deposition monitoring mostly concentrates on wet N_r deposition, while observations of dry N_r deposition are relatively scarce especially for surface HNO_3 and NH_4^+ and NO_3^-. Second, most observation networks focus on a few years or a certain period of time, leading to the lack of long-term continuously monitoring on both wet and dry N_r deposition. More importantly, the global N_r deposition monitoring network has not been established, and the sampling standards in different regions are not unified. These outline the potential room for improvement of ground-based N_r deposition monitoring.

2.2 Atmospheric Chemistry Transport Model (ACTM) Simulation

An ACTM can simulate N_r deposition at regional or global scales through explicitly representing the physical and chemical processes of atmospheric N_r components (Zhao et al., 2017;Zhang et al., 2012). Wet N_r deposition flux is parameterized as in-cloud, under-cloud and precipitation scavenging (Amos et al., 2012;Levine and Schwartz, 1982;Liu et al., 2001;Mari et al., 2000), while dry deposition flux can be obtained as the product of surface N_r concentration and V_d, which is typically parameterized as a network of resistances (Wesely and Hicks, 1977). Based on the integrated results of 11 models of HTAP (hemispheric transport of air pollution), Tan

et al. found that about 76%-83% of the ACTM's simulation results were ±50% of the monitoring values, and the modeling results underestimated the wet deposition of NH_4^+ and NO_3^- over Europe and East Asia, and overestimated the wet deposition of NO_3^- over the eastern US (Tan et al., 2018). Though regional ACTMs can be configured at very high horizontal resolution (e.g., 1×1 km^2) (Kuik et al., 2016), the horizontal resolution of global ACTMs are relatively coarse (1°×1°-5°×4°) (Williams et al., 2017), which cannot indicate the local pattern of N_r deposition. On the other hand, the N_r emission inventory used to drive an ACTM is highly uncertain, with the uncertainty of the NO_x emission at about ±30-40%, and that of NH_3 emission at about ±30-80% (Zhang et al., 2009;Cao et al., 2011).

2.3 Satellite-based Estimation of Surface N_r Concentration and Deposition

Satellite observation has wide spatial coverages and high resolution, and is spatiotemporally continuous. Atmospheric NO_2 and NH_3 columns can be derived from satellite measurements with relatively high accuracy (Van Damme et al., 2014a;Boersma et al., 2011), providing a new perspective about atmospheric N_r abundance.

Satellite instruments that can monitor NO_2 in the atmosphere include GOME (Global Ozone Monitoring Experience), SCIAMACHY (SCanning Imaging Absorption SpectroMeter for Atmospheric ChartographY), OMI (Ozone Monitoring Instrument), GOME-2 (Global Ozone Monitoring Experience-2). Some scholars applied satellite NO_2 columns to estimate the surface NO_2 concentration, and then dry NO_2 deposition by combining the surface NO_2 concentration and modeled V_d. Cheng et al. established a statistical model to estimate the surface NO_2 concentration based on the SCIAMACHY NO_2 columns, and then estimated the dry deposition of NO_2 over eastern China (Cheng et al., 2013). This method used the simple linear model and did

not consider the vertical profiles of NO_2 (Cheng et al., 2013). Lu et al. established a multivariate linear regression model based on the SCIAMACHY and GOME NO_2 columns, meteorological data and ground-based monitoring N_r deposition, and then estimated the global total N_r deposition (Lu et al., 2013). Lu et al. could not distinguish the contribution of dry and wet N_r deposition using the multivariate linear regression model (Lu et al., 2013). Jia et al. established a simple linear regression model based on OMI tropospheric NO_2 column and ground-based surface N_r concentration, and then estimated the total amounts of dry N_r deposition (Jia et al., 2016). Jia et al. used OMI tropospheric NO_2 column to estimate the dry deposition of reduced N_r deposition (NH_3 and NH_4^+), which could also bring great errors since the OMI NO_2 column could not indicate the NH_3 emission. These studies highlight the problem of using only NO_2 columns to derive total N_r deposition, that NO_2 columns give us highly limited information about the abundance of reduced N_r (NH_3 and NH_4^+).

Lamsal et al. first used the relationship between the NO_2 column and surface NO_2 concentration at the bottom layer simulated by an ACTM to convert OMI NO_2 column to surface NO_2 concentration (Lamsal et al., 2008). A series of works (Lamsal et al., 2013;Nowlan et al., 2014;Kharol et al., 2018) have effectively estimated regional and global surface NO_2 concentration using satellite NO_2 column combining with ACTM-derived relationship between the NO_2 column and surface NO_2 concentration simulated. It is worth mentioning that Nowlan et al. applied OMI NO_2 column to obtain the global dry NO_2 deposition during 2005-2007 for the first time (Nowlan et al., 2014). However, using satellite NO_2 column and ACTM-derived relationship between the NO_2 column and surface NO_2 concentration may lead to an underestimation of surface NO_2 concentration. Kharol et al. found that the

199 satellite-derived surface NO_2 concentration using the above method is only half of the
200 observed values (Kharol et al., 2015). To resolve such potential underestimation,
201 Larkin et al. established a statistical relationship between the satellite-derived and
202 ground measured surface NO_2 concentration, and then calibrated the satellite-derived
203 surface NO_2 concentration using the established relationship (Larkin et al., 2017).
204 Some researchers also estimated other N_r components (such as particulate NO_3^-)
205 based on satellite NO_2 column. Based on the linear model between NO_2, NO_3^-, HNO_3
206 obtained by ground-based measurements, Jia et al. calculated the surface NO_3^- and
207 HNO_3 concentration using satellite-derived surface NO_2 concentration and their
208 relationship (Jia et al., 2016). Geddes et al. reconstructed the NO_x emission data by
209 using the satellite NO_2 column, and then estimated the global NO_x deposition by an
210 ACTM, but the spatial resolution of global NO_x deposition remains low (2 °×2.5 °),
211 failing to exploit the higher resolution of satellite observation (Geddes and Martin,
212 2017).
213 Comparing with NO_2, the development of satellite NH_3 monitoring is relatively late.
214 Atmospheric NH_3 was first detected by the TES in Beijing and Los Angeles (Beer et
215 al., 2008). The IASI sensor also detected atmospheric NH_3 from a biomass burning
216 event in Greece (Coheur et al., 2009). Subsequently, many scholars began to develop
217 more reliable satellite NH_3 column retrievals (Whitburn et al., 2016;Van Damme et al.,
218 2014a), validate the satellite-retrieved NH_3 column with the ground-based observation
219 (Van Damme et al., 2014a;Dammers et al., 2016;Li et al., 2017), and compare the
220 satellite NH_3 column with the aircraft measured NH_3 column (Van Damme et al.,
221 2014b;Whitburn et al., 2016). In recent years, some scholars have carried out the
222 works of estimating surface NH_3 concentration based on satellite NH_3 column. Liu et
223 al. obtained the satellite-derived surface NH_3 concentration in China based on the

IASI NH_3 column coupled with an ACTM, and deepened the understanding of the spatial pattern of surface NH_3 concentration in China (Liu et al., 2017b). Similarly, Graaf et al. carried out the relevant work in Europe based on the IASI NH_3 column coupled with an ACTM, and estimated the dry NH_3 deposition in West Europe (Van der Graaf et al., 2018). Jia et al. first constructed the linear model between surface NO_2 and NH_4^+ concentration based on ground monitoring data, and then calculated the NH_4^+ concentration using satellite-derived surface NO_2 concentration and their relationship (Jia et al., 2016). However, as the emission sources of NO_x (mainly from transportation and energy sectors) and NH_3 (mainly from agricultural sector) are different (Hoesly et al., 2018), the linear model between surface NO_2 and NH_4^+ concentration may lead to large uncertainties in estimating the global NH_4^+ concentration. There is still no report about the satellite-derived dry and wet reduced N_r deposition using satellite NH_3 column at a global scale. As reduced N_r plays an important role in total N_r deposition, satellite NH_3 should be better utilized to help estimate reduced N_r deposition.

2.4 Problems in Estimating Global N_r Deposition

The spatial coverage of ground monitoring sites focusing on N_r deposition is still not adequate, and the monitoring standards and specifications in different regions of the world are not consistent, presenting a barrier to integrating different regional monitoring data. Large uncertainties exist in N_r emission inventory used to drive the ACTMs, and the spatial resolution of the modeled N_r deposition by ACTMs is coarse. Using satellite monitoring data to estimate surface N_r concentration and deposition is still in its infancy, especially for reduced N_r.

Some scholars tried to use satellite NO_2 and NH_3 column to estimate the surface N_r concentration and dry N_r deposition. However, there are relatively few studies on

estimating wet N_r deposition. In addition, the development of satellite monitoring for NH_3 in the atmosphere is relatively late (compared with NO_2). At present, IASI NH_3 data have been widely used, while the effective measurements of TES are less than IASI; CrIS and AIRS NH_3 column products are still under development. There are three main concerns in high-resolution estimation of surface N_r concentration and deposition based on satellite N_r observation. (1) How to effectively couple the satellite high-resolution NO_2 and NH_3 column data with the vertical profiles simulated by an ACTM, and then estimates the surface N_r concentrations? This step is the key to simulate the dry N_r deposition. (2) How to construct a model for estimating dry N_r deposition including all major N_r species based on satellite NO_2 and NH_3 column, and then estimates the dry N_r deposition at a high spatial resolution? (3) How to combine the high-resolution satellite NO_2 and NH_3 column data and ground-based monitoring data to construct wet N_r deposition models, and then estimate the wet N_r deposition at a high spatial resolution?

3. Framework of Estimating Surface N_r Concentration and Deposition Using Satellite Observation

Previous studies using satellite observation to estimate surface N_r concentration and deposition only focused on one or several N_r components, but not including all N_r components, which were decentralized, unsystematic and incomplete. Here we give a framework of using satellite observation to estimate surface N_r concentration and deposition as shown in **Fig. 1** based on recent advances.

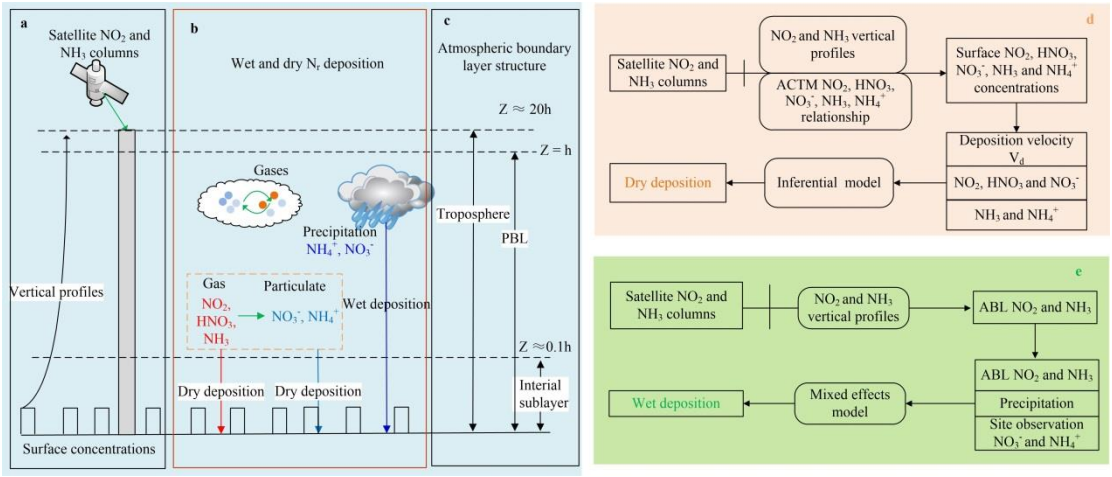

Fig. 1 Schematic diagram of dry and wet N_r deposition. (a) indicates satellite observed NO_2 and NH_3 column, and the vertical profiles by an ACTM; (b) shows dry and wet N_r deposition including the major N_r species (gaseous NO_2, HNO_3, NH_3, particulate NO_3^- and NH_4^+, as well as wet NO_3^- and NH_4^+ in precipitation); (c) illustrates atmospheric vertical structures including the troposphere (satellite observation), atmospheric boundary layer (ABL), interfacial sub-layer; (d) and (e) represent procedures of calculating the dry and wet N_r deposition.

3.1 Conversion of Satellite NO_2 and NH_3 Column to Surface N_r Concentration

An ACTM can simulate the vertical profiles of NO_2 and NH_3 with multiple layers from the surface to the troposphere. For example, the GEOS-Chem ACTM includes 47 vertical layers from the earth surface to the top of the stratosphere. Most previous studies estimated the ratio of surface N_r concentration (at the first layer) to total columns by an ACTM, and then multiply the ratio by satellite columns to estimate satellite-derived surface concentration (Geddes et al., 2016;Graaf et al., 2018;Nowlan et al., 2014).

Another approach tries to fit general vertical profiles of NO_2 and NH_3 (Zhang et al., 2017;Liu et al., 2017b;Liu et al., 2017c), and then estimate the ratio of N_r concentration at any height to total N_r columns, and finally multiply the ratio by satellite NO_2 and NH_3 columns. This approach has an advantage compared with the previous one for that NO_2 and NH_3 concentration at all altitude included in ACTM simulations can be estimated. Satellite NO_2 and NH_3 column data had no vertical profiles. Surface NO_2 and NH_3 concentration was estimated by modeled NO_2 and

293 NH_3 vertical profiles from the CTM. The Gaussian model was constructed to fit the
294 multiple layers' NO_2 and NH_3 concentrations with the altitude. The constructed
295 Gaussian model has general rules, appropriate for converting satellite columns to
296 surface concentration simply.
297 Taking the estimation of surface NO_2 concentration using the latter approach as an
298 example, the methods and steps are introduced in the following.
299 Step 1: Calculate the monthly mean NO_2 concentrations at all layers simulated by an
300 ACTM.
301 Step 2: Construct the vertical profile function of NO_2. Multiple Gaussian functions are
302 used to fit the vertical distribution of NO_2 based on the monthly NO_2 concentrations at
303 all layers calculated in Step 1, in which the independent variable is the height
304 (altitude), and the dependent variable is NO_2 concentration at a certain height.
305 The basic form of single Gaussian function is (Zhang et al., 2017;Liu et al., 2017b;Liu
306 et al., 2017c;Whitburn et al., 2016):

307 $$\rho = \rho_{max} e^{-(\frac{Z-Z_0}{\sigma})^2} \quad (1)$$

308 where Z is the height of a layer in the ACTM; ρ_{max}, Z_o and σ are the maximum NO_2
309 concentration, the corresponding height with the maximum NO_2 concentration and the
310 thickness of NO_2 concentration layer (one standard error of Gaussian function).
311 There are two basic forms of profile shapes of NO_2: (1) NO_2 concentration reaches the
312 maximum concentration when reaching a certain height ($Z_o \neq 0$). As the height
313 increases, the NO_2 concentration begins to decline; (2) NO_2 concentration is basically
314 concentrated on the earth surface ($Z_o=0$). These two cases are the ideal state of the
315 vertical distribution of NO_2 concentration. In reality, single Gaussian fitting may not
316 capture the vertical distribution of NO_2 well. To improve the accuracy of fitting, the
317 sum of multiple Gaussian functions can be used (Liu et al., 2019):

$$\rho(Z) = \sum_{i=1}^{n} \rho_{max,i} e^{-(\frac{Z-Z_{0,i}}{\sigma_i})^2} \quad (2)$$

Step 3: Calculate the ratio of NO_2 concentration at the height of h_G to total columns ($\int_0^{h_{trop}} \rho(Z)\,dx$), and then multiply the ratio by satellite column (S_{trop}). The satellite-derived N_r concentration at the height of h_G can be calculated as:

$$S_{G\_NO2} = S_{trop} \times \frac{\rho(h_G)}{\int_0^{h_{trop}} \rho(Z)dx} \quad (3)$$

Step 4: Convert the instantaneous satellite-derived surface NO_2 concentration (S_{G_NO2}) to daily average ($S_{G\_NO2}*$) using the ratio of average surface NO_2 concentration (G_{ACTM}^{1-24}) to that at satellite overpass time ($G_{ACTM}^{overpass}$) by an ACTM (Liu et al., 2020):

$$S_{G\_NO2}* = \frac{G_{ACTM}^{1-24}}{G_{ACTM}^{overpass}} \times S_{G\_NO2} \quad (4)$$

The method for estimating the surface NH_3 concentration ($S_{G\_NH3}*$) is similar to that for estimating the surface NO_2 concentration.

3.2 Estimating Surface Concentration of Other N_r Species

At present, only NO_2 and NH_3 column can be retrieved reliably, and there are no reliable satellite retrievals of HNO_3, NH_4^+ and NO_3^-. For example, the IASI HNO_3 product is still in the stage of data development and verification (Ronsmans et al., 2016). Previous studies firstly derive the relationship between N_r species by an ACTM or by ground-based measurements, and then use the relationship to convert satellite-derived surface NO_2 and NH_3 concentration ($S_{G\_NH3}*$) to HNO_3, NH_4^+ and NO_3^- concentrations:

$$\begin{cases} G_{S\_NO3} = S_{G\_NO2} * \times \frac{G_{ACTM\_NO3}}{G_{ACTM\_NO2}} \\ G_{S\_HNO3} = S_{G\_NO2} * \times \frac{G_{ACTM\_HNO3}}{G_{ACTM\_NO2}} \\ G_{S\_NH4} = S_{G\_NH3} * \times \frac{G_{ACTM\_NH4}}{G_{ACTM\_NH3}} \end{cases} \quad (5)$$

$\frac{G_{ACTM\_NO3}}{G_{ACTM\_NO2}}$, $\frac{G_{ACTM\_HNO3}}{G_{ACTM\_NO2}}$, $\frac{G_{ACTM\_NH4}}{G_{ACTM\_NH3}}$ is the estimated ratio of between NO_2 and NO_3^-,

NO_2 and HNO_3, NH_3 and NH_4^+.

3.3 Dry Deposition of N_r

The resistance of dry N_r deposition mainly comes from three aspects: aerodynamic resistance (R_a), quasi laminar sub-layer resistance (R_b) and canopy resistance (R_c). The V_d can be expressed as

$$V_d = \frac{1}{R_a + R_b + R_c} + v_g \quad (6)$$

V_g is gravitational settling velocity. For gases, the V_g is negligible (V_g=0).

Dry NO_2, NO_3^-, HNO_3, and NH_4^+ deposition can be calculated by:

$$F = G_S \times V_d \quad (7)$$

Unlike above species, NH_3 is bi-directional, presenting both upward and downward fluxes. There is a so-called "canopy compensation point" (C_o) controlling dry NH_3 deposition. Dry NH_3 deposition can be calculated by:

$$F = (G_{S\_NH3} - C_o) \times V_d \quad (8)$$

The calculation of C_o is very complex including the leaf stomatal and soil emission potentials related to the meteorological factors, the plant growth stage and the canopy type. The satellite-based methods usually neglected this complex process and set C_o as zero (Graaf et al., 2018;Kharol et al., 2018) or set fixed values in each land use type based on ground-based measurements (Jia et al., 2016).

3.4 Wet Deposition of N_r

The satellite-based estimation of wet N_r deposition can be simplified as the product of the concentration of N_r (C), precipitation (P) and scavenging coefficient (w) (Pan et al., 2012). Satellite NO_2 and NH_3 can be used to indicate the oxidized N_r and reduced N_r; precipitation (P) can be obtained from ground monitoring data or reanalysis data (such as NCEP). However, the scavenging coefficient (w) is usually highly uncertain. To improve the accuracy of estimation, a mixed-effects model (Liu et al.,

2017a;Zhang et al., 2018) is proposed to build the relationship between satellite NO_2 and NH_3, precipitation and ground monitoring wet N_r deposition:

$$WetN_{ij} = \alpha_j + \beta_i \times P_{ij} \times (S_{ABL})_{ij} + \varepsilon_{ij} \quad (9)$$

$$S_{ABL} = S_{trop} \times \frac{\int_0^{ABL} \rho(Z)dx}{\int_0^{h_{trop}} \rho(Z)dx} \quad (10)$$

$WetN_{ij}$ is wet NO_3^-N or NH_4^+-N deposition at month i and site j; $(S_{ABL})_{ij}$ is the atmospheric boundary layer (ABL) NO_2 or NH_3 columns at month i and site j; P_{ij} is precipitation at month i and site j; β_i and α_j are the slope and intercept of random effects, representing seasonal variability and spatial effects; ε_{ij} represents the random error at month i and site j. The mixed effects models were appropriate for estimating both wet NO_3^- and NH_4^+ deposition using the satellite observations.

The scavenging process of wet N_r deposition usually starts from the height of rainfall rather than the top of the troposphere, so it is more reasonable to use NO_2 and NH_3 column below the height of rainfall to build the wet N_r deposition model. The NO_2 and NH_3 column within ABL is used to build the wet deposition model since precipitation height is close to the height of the ABL (generally less than 2-3 km).

4. Satellite-derived Surface N_r Concentration and Deposition

4.1 Surface NO_2 Concentration and Oxidized N_r Deposition

The spatial resolutions of global ACTMs and therefore modeled surface N_r concentration are very coarse (for example, the spatial resolution of the global version of GEOS-Chem is $2^o \times 2.5^o$). Thus it can be hard to estimate surface N_r concentration and deposition at a fine resolution at a global scale by ACTMs alone. Instead, the satellite N_r retrievals have a high spatial resolution and can reveal more spatial details than ACTM simulations.

Cheng et al. and Jia et al. established a linear model between the surface NO_2

concentration and NO_2 column by assuming the ratio of the surface NO_2 concentration to the tropospheric NO_2 column to be fixed, and then used the linear model to convert satellite NO_2 columns to surface NO_2 concentration, and finally estimated dry NO_2 deposition using the inferential method (Cheng et al., 2013;Jia et al., 2016). However, these statistical methods are highly dependent on the ground-based measurements, and the established linear models may be not effective over regions with few monitoring sites.

A comprehensive study (Nowlan et al., 2014) estimated global surface NO_2 concentration during 2005-2007 by multiplying OMI tropospheric NO_2 columns by the ACTM-modeled ratio between surface NO_2 concentration and tropospheric column (**Fig. 2**). Nowlan et al. also estimated dry NO_2 deposition using the OMI-derived surface NO_2 concentration combining the modeled V_d during 2005-2007 (Nowlan et al., 2014). This approach followed an earlier study (Lamsal et al., 2008), that focus on North America. As reported by Lamsal et al., the satellite-derived surface NO_2 concentration was generally lower than ground-based NO_2 observations, ranging from -17% to -36% in North America (Lamsal et al., 2008). Kharol et al. used a similar method and found the satellite-derived surface NO_2 concentration was only half of the ground-measured values in North America (Kharol et al., 2015).

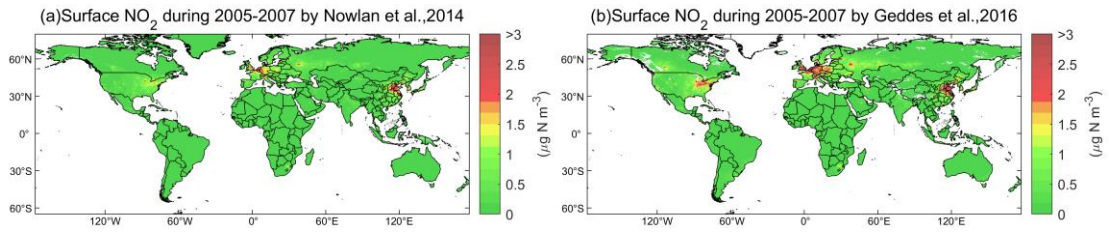

Fig. 2 Satellite-derived surface NO_2 concentration during 2005-2007 by Nowlan et al. (Nowlan et al., 2014) (a) and by Geddes et al. (Geddes et al., 2016) (b). We gained the surface NO_2 concentration by Nowlan et al. (Nowlan et al., 2014) and by Geddes et al. (Geddes et al., 2016) at the web: http://fizz.phys.dal.ca/~atmos/martin/?page_id=232.

Geddes et al. followed previous studies, and used NO_2 column from the GOME, SCIAMACHY, and GOME-2 to estimate surface NO_2 concentration (Geddes et al.,

2016). Although Geddes et al. did not evaluate their results with ground-based observation (Geddes et al., 2016), it is obvious that their surface NO_2 estimates were higher than Nowlan's estimates based on OMI (Nowlan et al., 2014) (**Fig. 2**). This may be because the OMI-derived NO_2 column is much lower than that derived by GOME, SCIAMACHY, and GOME-2, especially over polluted regions. For example, in China, the OMI NO_2 column is about 30% lower than that of SCIAMACHY and GOME-2 consistently (**Fig. 3**).

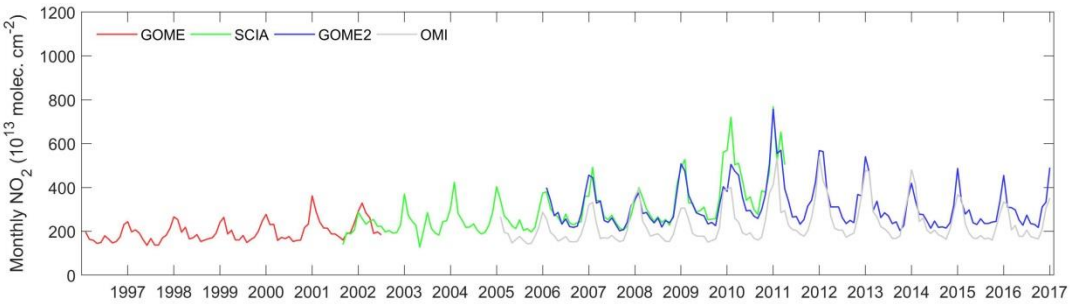

Fig. 3 An example of the time series of monthly NO_2 column retrieved by GOME, SCIAMACHY, GOME2 and OMI in China. We obtained the GOME, SCIAMACHY, GOME2 and OMI data from http://www.temis.nl/airpollution/no2.html.

Larkin et al. established a land-use regression model to estimate global surface NO_2 concentration by combining satellite-derived surface NO_2 concentration by Geddes et al. and ground-based annual NO_2 measurements (Geddes et al., 2016;Larkin et al., 2017). The study by Larkin et al. can be considered as using the ground-based annual measurements to adjust the satellite-derived surface NO_2 concentration by Geddes et al. (Geddes et al., 2016;Larkin et al., 2017), which helped reduce the discrepancy between satellite-derived and ground-measured NO_2 concentration. The regression model captured 54% of global NO_2 variation, with an absolute error of 2.32 μg N m^{-3}. Zhang et al. followed the framework in **Sect. 3** to estimate the OMI-derived surface NO_2 concentration (at ~50 m) in China, and found good agreement with ground-based surface NO_2 concentration from the NNDMN at yearly scale (slope=1.00, R^2=0.89) (Zhang et al., 2017). The methods by Zhang et al. can also generate OMI-derived NO_2

concentration at any height by the constructed NO_2 vertical profile (Zhang et al., 2017). Zhang et al. also estimated dry NO_2 deposition using the OMI-derived surface NO_2 concentration combining the modeled V_d during 2005-2016 (Zhang et al., 2017). Based on Zhang's estimates, the Gaussian function can well simulate the vertical distribution of NO_2 from an ACTM (MOZART) (Emmons et al., 2010) with 99.64% of the grids having R^2 values higher than 0.99. This suggests that the ACTM-simulated vertical distribution of NO_2 has a general pattern, which can be emulated by Gaussian functions. Once a vertical profile was constructed, it can be easily used to estimate NO_2 concentration at any height.

In this study, we used the framework in **Sect. 3** to estimate the OMI-derived surface NO_2 concentration globally. To validate the OMI-derived surface NO_2 concentrations, ground-measured surface NO_2 concentration in China, the US and Europe in 2014 was collected (**Fig. 4**). The total number of NO_2 observations in China, the US and Europe are 43, 373 and 88 respectively. The OMI-derived annual average for all sites was 3.74 μg N m^{-3}, which was close to the measured average (3.06 μg N m^{-3}). The R^2 between OMI-derived surface NO_2 concentrations and ground-based NO_2 measurements was 0.75 and the RMSE was 1.23 μg N m^{-3} (**Fig. 5**), which is better than the modeling results by the GEOS-Chem ACTM (R^2=0.43, RMSE=1.93 μg N m^{-3}). We did not simply use the relationship between the NO_2 column and surface NO_2 concentration from the CTM. As presented in the methods, we can estimate surface NO_2 concentration at any height by using the Gaussian function. We used the surface NO_2 concentration at a certain height (~60 m) which best matched with the ground-based measurements. Satellite-based methods have the advantages of spatiotemporally continuous monitoring N_r at a higher resolution, which helps alleviate the problem of the coarse resolution of ACTMs in estimating N_r

concentration and deposition. The readers can use any satellite data (GOME, SCIAMACHY, GOME2 or OMI) combining the Gaussian function to estimate surface NO_2 concentrations. They can use surface NO_2 concentrations at a certain height which best matched with the ground-based measurements. The key is not selecting which satellite data we should use, but determining which height of surface NO_2 concentrations that better matched with the ground-based measurements by Gaussian function.

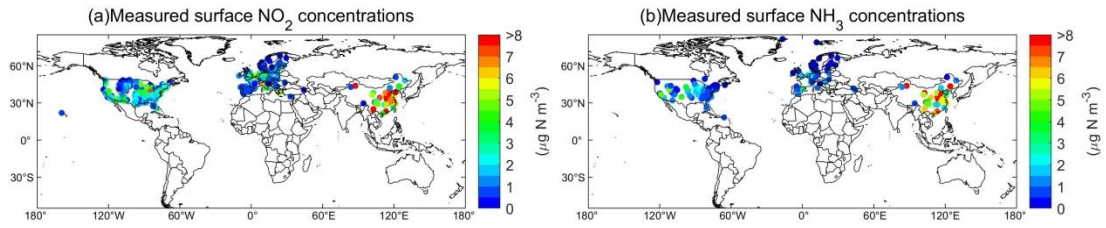

Fig. 4 Spatial distribution of measured surface NO_2 and NH_3 concentrations in 2014. For NO_2 (a), the measured data in China, the US and Europe were obtained from the NNDMN, US-EPA and EMEP, respectively; for NH_3 (b), the measured data in China, the US and Europe were obtained from the NNDMN, US-AMoN and EMEP, respectively

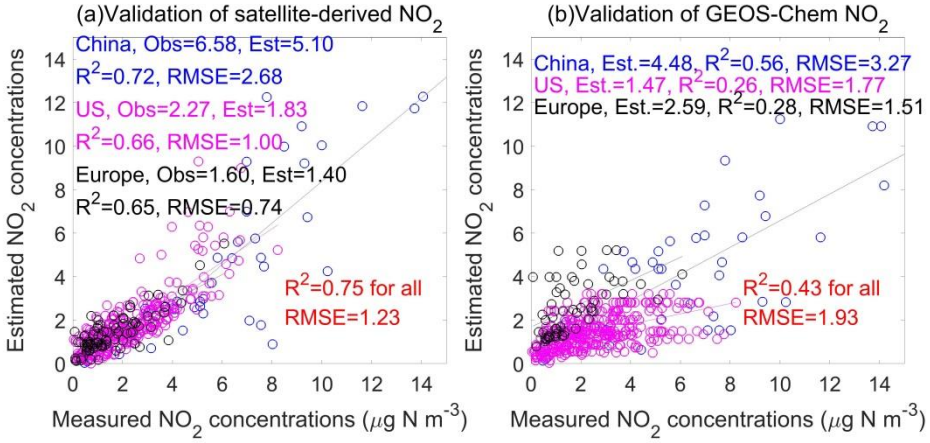

Fig. 5 Comparison between annual mean satellite-derived and ground-measured surface NO_2 concentrations (a), and comparison between annual mean modeled (by an ACTM as GEOS-Chem) and ground-measured surface NO_2 concentrations (b). The ground-based monitoring sites are shown in **Fig. 4**.

For NO_3^- and HNO_3, previous studies firstly constructed the relationship between NO_2, NO_3^- and HNO_3, and found a relatively high linear relationship between NO_2, NO_3^-, and HNO_3 at a monthly or yearly scale. For example, Jia et al. found a linear

485 relationship between NO_2 and NO_3^-, HNO_3 concentration at annual scale (R^2=0.70)
486 (Jia et al., 2016). Similarly, based on the ground-based measurements in the NNDMN,
487 a high correlation was found between surface NO_2 and NO_3^- concentration at monthly
488 or annual timescales (**Fig. 6**) (Liu et al., 2017c). Using these linear relationships and
489 satellite-derived surface NO_2 concentration, the annual mean surface NO_3^- and HNO_3
490 can be estimated. Alternatively, the relationship of NO_2, NO_3^- and HNO_3 can also be
491 modeled by an ACTM. For example, a strong relationship of tropospheric NO_2, NO_3^-
492 and HNO_3 column was simulated over all months by an ACTM, with the correlation
493 ranging from 0.69 to 0.91 (Liu et al., 2017a). But, over shorter timescales, the
494 relationship between NO_2, NO_3^- and HNO_3 may be nonlinear, which we should be
495 cautious about when estimating surface NO_3^- and HNO_3 concentration from NO_2
496 concentration.

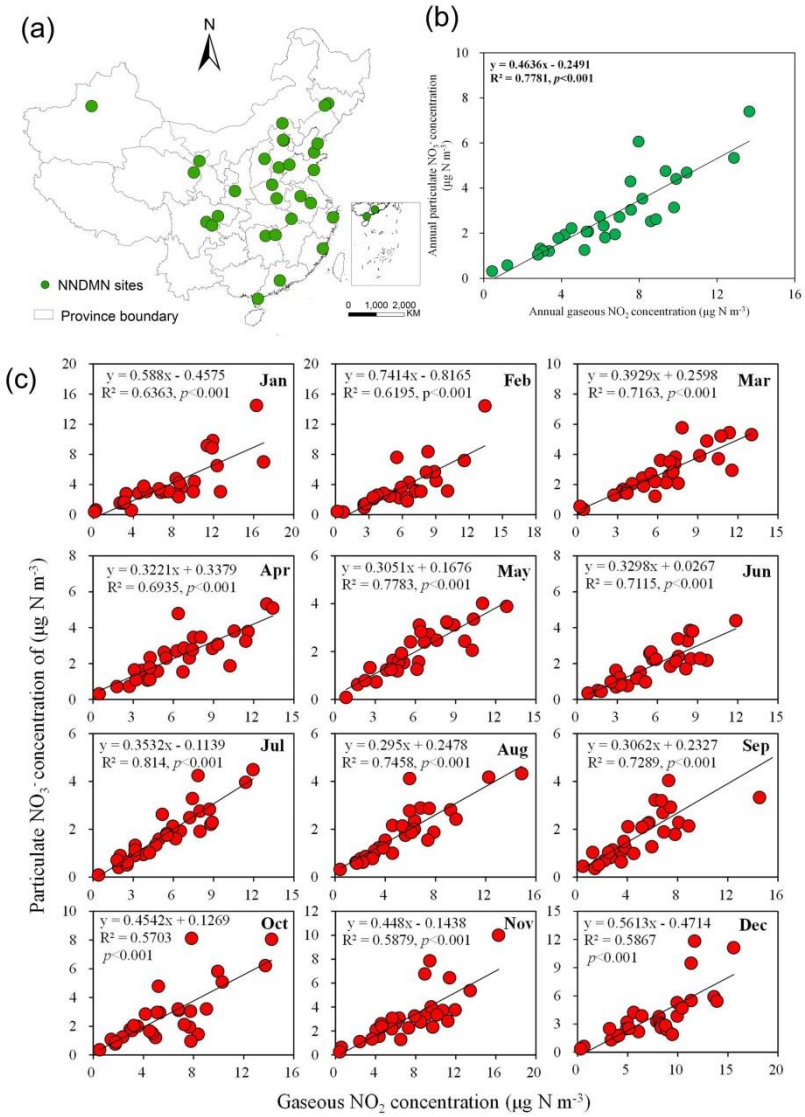

Fig. 6 Correlation between surface NO_2 and particulate NO_3^- concentration in the NNDMN at annual and monthly scales, which were adopted from our previous study (Liu et al., 2017c). (a) indicates the spatial locations of monitoring sites in the NNDMN; (b) and (c) represent yearly and monthly relationship between surface NO_2 and particulate NO_3^- concentration, respectively.

For the wet N_r deposition, Liu et al. followed the framework in **Sect. 3** to estimate wet nitrate deposition using ABL NO_2 columns derived from OMI NO_2 column and NO_2 vertical profile from an ACTM (MOZART), and precipitation by a mixed-effects model showing the proposed model can achieve high predictive power for monthly wet nitrate deposition over China (R=0.83, RMSE=0.72) (Liu et al., 2017a).

4.2 Surface NH_3 Concentration and Reduced N_r Deposition

With the development of atmospheric remote sensing of NH_3, some scholars have

estimated surface NH_3 concentration and dry NH_3 deposition based on the satellite NH_3 column data. Assuming the ratio between the surface NH_3 concentration to the NH_3 column was fixed, Yu et al. applied a linear model to convert satellite NH_3 columns to surface NH_3 concentration and estimated dry NH_3 deposition in China using the inferential method (Yu et al., 2019). But Yu et al. did not consider the spatial variability of the vertical profiles of NH_3 (Yu et al., 2019), which may cause a large uncertainty in estimating surface NH_3 concentration.

In Western Europe, Graaf et al. used the ratio of the surface NH_3 concentration (in the bottom layer) to total NH_3 column from an ACTM to convert the IASI NH_3 column to surface NH_3 concentration, and then estimated dry NH_3 deposition combining the modeled deposition velocity and IASI-derived surface NH_3 concentration (Graaf et al., 2018). Similarly, in North America, Kharol et al. estimated the dry NH_3 deposition by the CrIS-derived surface NH_3 concentration and deposition velocity of NH_3 (Kharol et al., 2018). They found a relatively high correlation (R=0.76) between the CrIS-derived surface NH_3 concentration and AMoN measurements during warm seasons (from April to September) in 2013 (**Fig. 7**). Over China, Liu et al. found a higher correlation (R=0.81) between IASI-derived surface NH_3 concentrations and the measured surface NH_3 concentrations than those from an ACTM (R=0.57, **Fig. 8**) (Liu et al., 2017b).

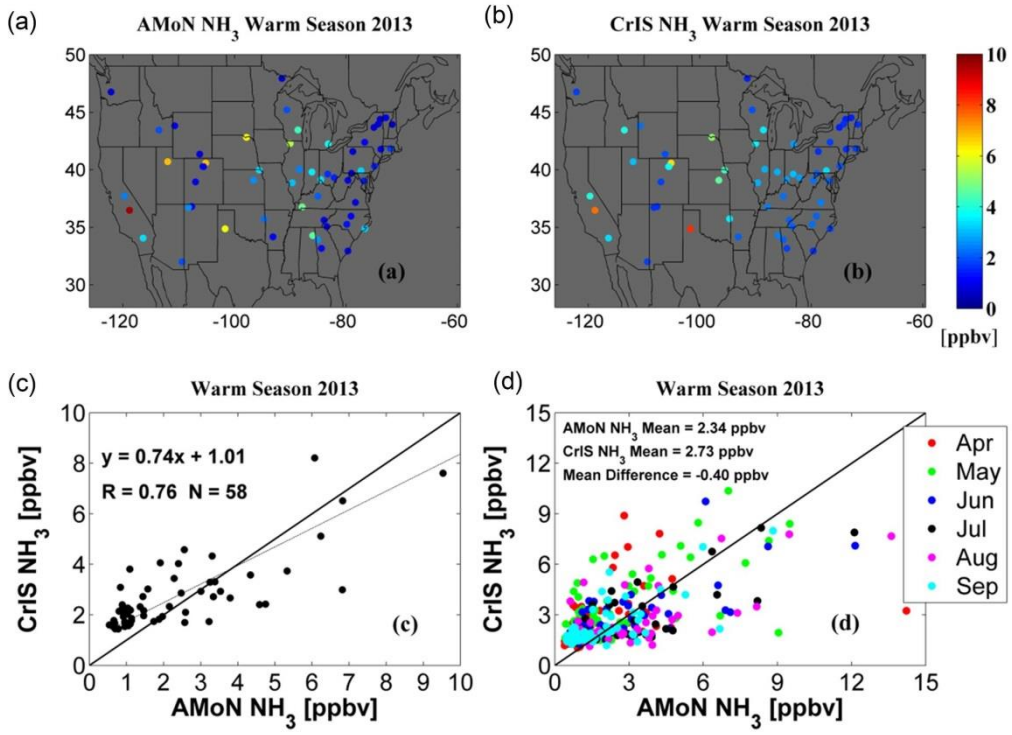

529

530 **Fig. 7** Comparisons of the measured surface NH_3 concentration by the AMoN and CrIS-derived
531 surface NH_3 concentration in the US during warm season (April-September) in 2013 (Kharol et al.,
532 2018). (a) and (b) indicate measured and CrIS-derived surface NH_3 concentration at the AMoN
533 sites, respectively; (c) represents the comparison of averaged surface NH_3 concentration during
534 warm months between CrIS-derived estimates and measurements, while (d) indicates the
535 comparison of monthly surface NH_3 concentration between CrIS-derived estimates and
536 measurements.
537

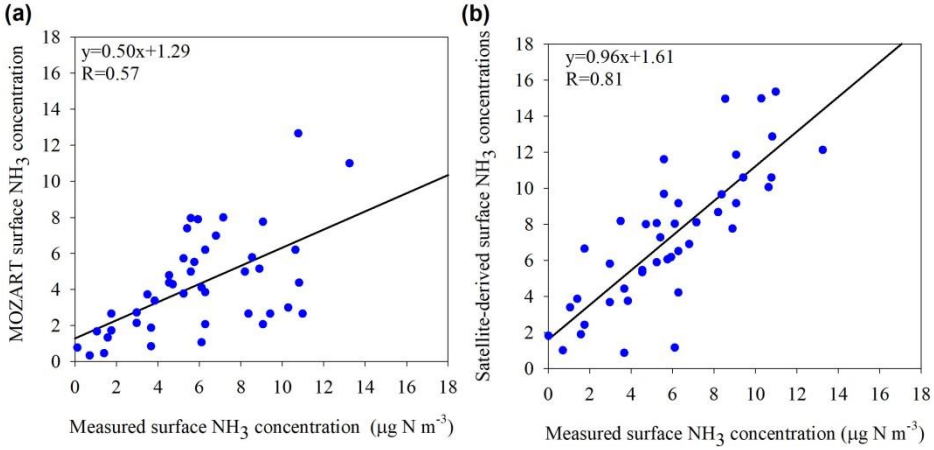

538

539 **Fig. 8** Comparisons of the measured surface NH_3 concentration with IASI-derived surface NH_3
540 concentration at the NNDMN sites over China (Liu et al., 2017b). (a) indicates the comparison of
541 measured and modeled surface NH_3 concentration from an ACTM (MOZART), and (b) represents
542 the comparison of the measured and IASI-derived surface NH_3 concentration.
543

544 Liu et al. followed the framework in **Sect. 3** to estimate the IASI-derived surface NH_3

545 concentration (at the middle height of the first layer by an ACTM) (**Fig. 9**), and found

a good agreement with ground-based surface NH_3 concentration (Liu et al., 2019). The correlation between the measured and satellite-derived annual mean surface NH_3 concentrations over all sites was 0.87 as shown in **Fig. 10**, while the average satellite-derived and ground-measured surface NH_3 concentration was 2.52 and 2.51 μg N m^{-3} in 2014 at the monitoring sites, respectively. The satellite-derived estimates achieved a better accuracy (R^2=0.76, RMSE = 1.50 μg N m^{-3}) than an ACTM (GEOS-Chem, R^2=0.54, RMSE = 2.14 μg N m^{-3}). The satellite NH_3 retrievals were affected by the detection limits of the satellite instruments and thermal contrast. Higher correlation over China than other regions for the satellite estimates was linked to the detection limits by the instruments and thermal contrast (Liu et al., 2019). Higher accuracy could be gained with higher thermal contrast and NH_3 abundance. Instead, the uncertainties of NH_3 retrievals would be higher with lower thermal contrast and NH_3 abundance.

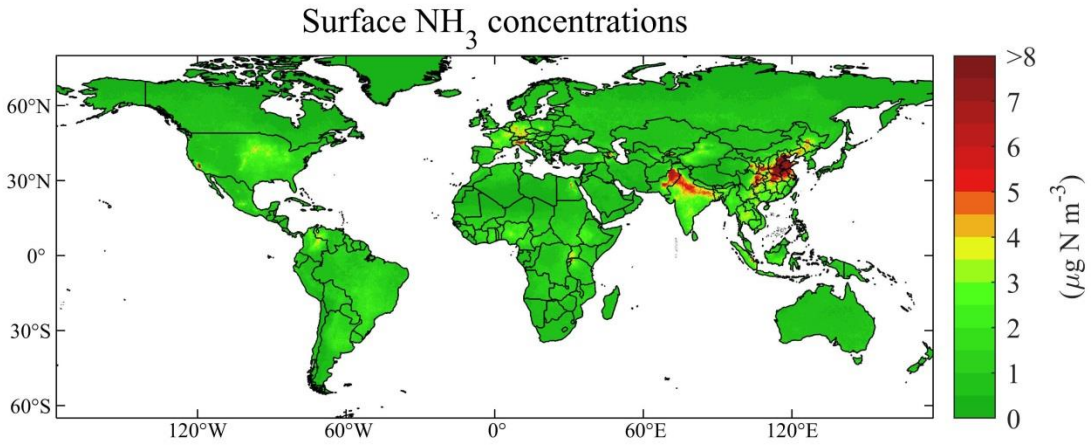

Fig. 9 Spatially satellite-based surface NH_3 estimates in 2014 (Liu et al., 2019). The global surface NH_3 concentration datasets have been released on the website: https://zenodo.org/record/3546517#.Xj6I4GgzY2w.

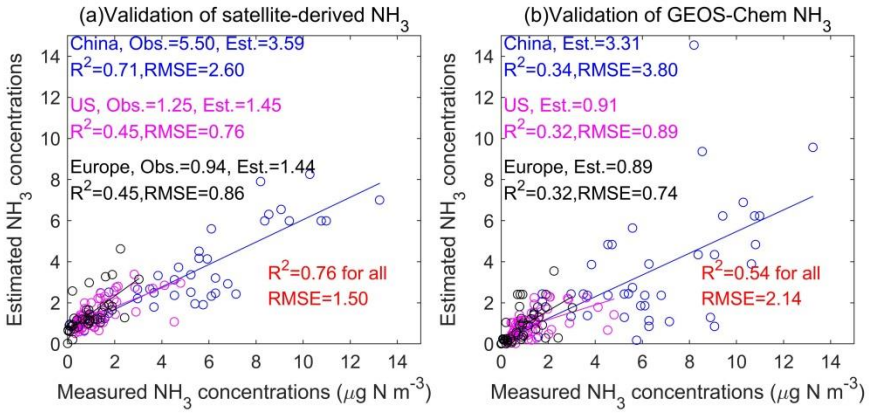

564

565 **Fig. 10** Comparison between yearly satellite-based and measured surface NH_3 concentrations (a),
566 and comparison between yearly modeling (by an ACTM as GEOS-Chem) and measured surface
567 NH_3 concentrations (b) (Liu et al., 2019). The ground-based monitoring sites are shown in **Fig. 4**.
568

569 The proposed methods (Liu et al., 2019) can also estimate NH_3 concentration at any
570 height using the constructed vertical profile function of NH_3. The Gaussian function
571 can well emulate the vertical distribution of NH_3 from an ACTM outputs with 99% of
572 the grids having R^2 values higher than 0.90 (**Fig. 11**). This means, for regional and
573 global estimation, the vertical distribution of NH_3 concentration has a general pattern,
574 which can be mostly emulated by the Gaussian function. Once a global NH_3 vertical
575 profile was simulated, it can be easily used to estimate satellite-derived NH_3
576 concentration at any height. We can also estimate dry NH_3 deposition using the
577 IASI-derived surface NH_3 concentration combining the modeled V_d. For the dry
578 deposition, the uncertainty mainly came from the satellite-derived estimates using the
579 modeled vertical profiles. The uncertainty of vertical profiles modeled by the ACTM
580 mainly resulted from the chemical and transport mechanisms. We recommend using
581 the Gaussian function to determine the height of surface NO_2 and NH_3 concentrations
582 that best matched with the ground-based measurements. There may exist systematic
583 biases by simply using the relationship of NO_2 columns and surface concentration to
584 estimate satellite surface NO_2 concentrations. To date, there are still no studies

585 developing satellite-based methods to estimate the wet reduced N_r deposition on a
586 regional scale.

587 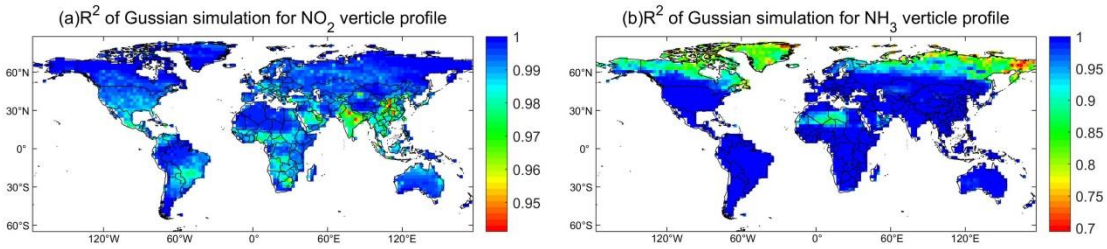

588 **Fig. 11** Spatial distributions of R^2 for Gaussian function by simulating NH_3 and NO_2 vertical
589 profiles. This is an example of Gaussian fitting using 47 layers' NH_3 and NO_2 concentration from
590 an ACTM (GEOS-Chem).
591

592 **5. Trends of Surface N_r Concentration and Deposition by Satellite-based**
593 **Methods**

594 The N_r concentration and deposition modeled by ACTMs are highly dependent on the
595 accuracy of input N_r emissions. The methods commonly used to estimate
596 anthropogenic N_r emissions are based on the data of human activities and emission
597 factors, which can be highly uncertain. The ACTM methods driven by N_r emission
598 inventory have relatively poor timeliness, and have limitations in monitoring the
599 recent trends of N_r deposition.

600 Satellite-based methods provide a simple, fast and relatively objective way to
601 monitoring N_r deposition at a high resolution, and less susceptible to the errors in the
602 assumptions that emission inventories are compiled based on, particularly the lack of
603 reliable data over developing countries (Crippa et al., 2018). With such advantages,
604 researchers developed the satellite-based methods to estimate surface N_r concentration,
605 deposition and even emissions. Satellite-based methods have advantages in
606 monitoring the recent trends of N_r deposition. Geddes et al. used NO_2 column from
607 the GOME, SCIAMACHY, and GOME-2 to estimate satellite-derived NO_x emissions,
608 and then used the calibrated NO_x emission inventory to drive an ACTM to simulate
609 the long-term oxidized N_r deposition globally (Geddes and Martin, 2017). They found

oxidized N_r deposition from 1996 to 2014 decreased by 60% in Eastern US, doubled in East China, and declined by 20% in Western Europe (**Fig. 12**). We use the datasets by Geddes et al. to calculate the trends of total oxidized N_r deposition during 1996-2014 (Geddes and Martin, 2017). It is obvious that two completely opposite trends exist: (1) in East China with a steep increase of higher than 0.5 kg N ha^{-1} y^{-1} and (2) East US with a steep decrease of lower than -0.5 kg N ha^{-1} y^{-1}. Although it is not a direct way to use satellite N_r observation to estimate N_r deposition, the method of estimating trends of N_r deposition by Geddes et al. can be considered effective since it took account of the changes of both NO_x emission and climate by an ACTM (Geddes and Martin, 2017).

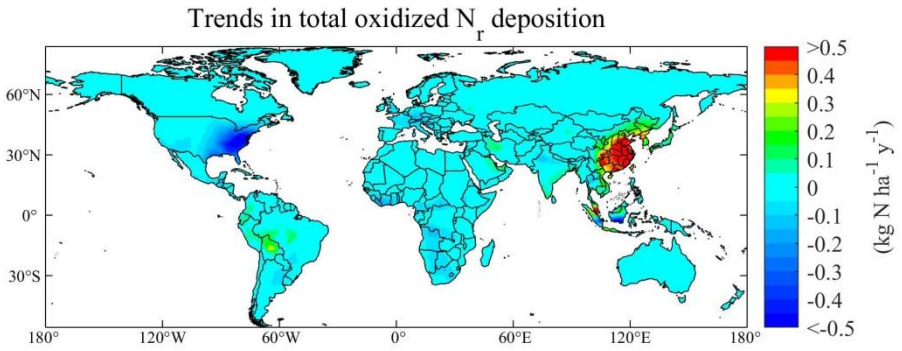

Fig. 12 Gridded annual changes of total oxidized N_r deposition simulated by GEOS-Chem constrained with GOME, SCIAMACHY, and GOME-2 NO_2 retrievals during 1996-2014 (Geddes and Martin, 2017). We gained the generated datasets (http://fizz.phys.dal.ca/~atmos/martin/?page_id=1520) by Geddes et al., and calculated the trends using the linear methods.

Some researchers developed a more direct way to infer the trends of surface N_r concentration and deposition. Geddes et al. presented a comprehensive long-term global surface NO_2 concentration estimate (at 0.1 ° resolution using an oversampling approach) between 1996 and 2012 by using NO_2 column from the GOME, SCIAMACHY, and GOME-2 (Geddes et al., 2016). The surface NO_2 concentration in North America (the US and Canada) decreased steeply, followed by Western Europe, Japan and South Korea, while approximately tripled in China and North Korea

(Geddes et al., 2016). Jia et al. established a simple linear regression model based on OMI NO_2 column and ground-based surface N_r concentration, and then estimated the trends of dry N_r deposition globally between 2005 and 2014 (Jia et al., 2016). They found that dry N_r deposition in Eastern China increased rapidly, while in the Eastern US, Western Europe, and Japan dry N_r deposition has decreased in recent decades.

We used the proposed framework to estimate the long-term surface NO_2 concentrations by OMI during 2005-2016. Note that the simulated profile function has a general rule, which can be well simulated by Gaussian function for any year (for our case during 2005-2016). The emission inventories should not affect the vertical profiles shapes using Gaussian function, but the transport and chemical mechanism in the CTM may affect the accuracy of the vertical profile distribution. The satellite-based methods did not need to rely on the accuracy of the statistical emission data. We split the time span of 2005-2016 into two periods: 2005-2011 and 2011-2016, as surface NO_2 concentration shows opposite trend in China in these two periods. The magnitudes of both growth and decline in surface NO_2 concentration in China are most pronounced worldwide in the two periods (**Fig. 13**). During 2005-2011, apart from Eastern China with the largest increase in surface NO_2 concentration, there are also several areas with increasing trends such as Northwest and East India (New Delhi and Orissa), Western Russia, Eastern Europe (Northern Italy), Western US (Colorado and Utah), Northwestern US (Seattle and Portland), Southwestern Canada (Vancouver, Edmonton, Calgary), Northeast Pakistan and Northwest Xinjiang (Urumqi). Notably, the biggest decreases in surface NO_2 concentration during 2005-2011 occurred in Eastern US and Western EU (North France, South England, and West German). During 2011-2016, due to the strict control of NO_x emissions, Eastern China had the largest decrease in surface NO_2 concentration than elsewhere worldwide, followed by

Western Xinjiang, Western Europe and some areas in Western Russia.

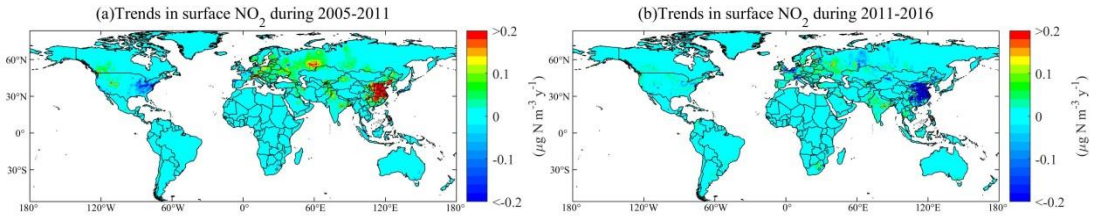

Fig. 13 Gridded annual changes in surface NO_2 concentrations gained by OMI retrievals during 2005-2011 (a) and during 2011-2016 (b) in this study. We have released the global surface NO_2 concentrations during 2005-2016 available at the website: https://zenodo.org/record/3546517#.Xj6I4GgzY2w.

Liu et al. estimated surface NH_3 concentration globally during 2008-2016 using satellite NH_3 retrievals by IASI (Liu et al., 2019). A large increase of surface NH_3 concentrations was found in Eastern China, followed by Northern Xinjiang province in China during 2008-2016 (**Fig. 14**). Satellite-based methods have been proven as an effective and unique way to monitoring the trends of global N_r concentration and deposition. To date, there are still few studies reporting the satellite-derived trends of reduced N_r deposition on a global scale.

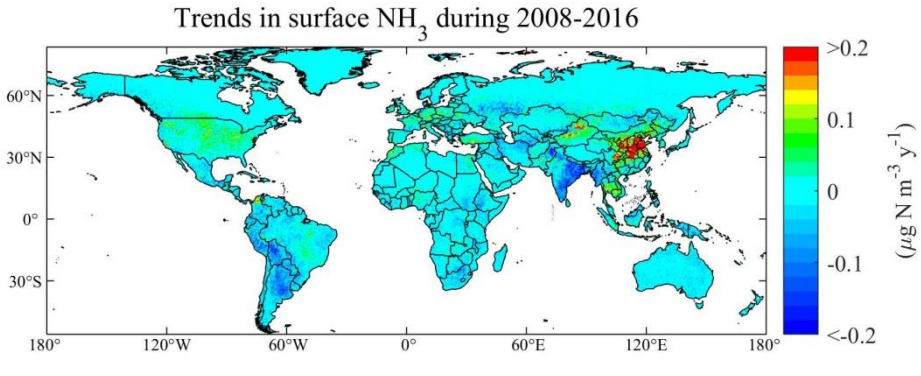

Fig. 14 Gridded annual changes in surface NH_3 concentrations gained by IASI retrievals during 2008-2016 (Liu et al., 2019). We have released the global surface NH_3 concentrations during 2008-2016 at the website: https://zenodo.org/record/3546517#.Xj6I4GgzY2w.

6. Remaining Challenges for Estimating N_r Deposition Using Satellite Observation

First, the reduced N_r deposition plays an important contribution to total N_r deposition. NH_3 exhibits bi-directional air-surface exchanges. The NH_3 compensation point

(Farquhar et al., 1980) is also an important and highly variable factor controlling dry NH_3 deposition (Schrader et al., 2016;Zhang et al., 2010). However, the current existing satellite-based methods did not consider this bi-directional air-surface exchange. It is important to better parameterize the NH_3 compensation point, and assess the effects of bi-directional air-surface exchanges on estimating the dry NH_3 deposition.

Second, the existing satellite-based methods to estimate N_r deposition used the ratio of the surface N_r concentration to the N_r column by an ACTM to convert satellite N_r column to surface N_r concentration. However, the calculated ratio (by an ACTM) and the satellite N_r column have different spatial resolutions, and previous studies usually applied the modeled ratio directly or interpolate the ratio into the resolution of satellite N_r column. This method assumes the relationship at coarse resolution by an ACTM can also be effective in fine resolution as satellite indicated. When regional studies are conducted, regional ACTMs coupled with another meteorological model (e.g. WRF-Chem, WRF-CMAQ) (Grell et al., 2005;Wong et al., 2012) can be configured to match the spatial resolution of satellite observation, but this is not as viable for global ACTMs (e.g. MOZART, GEOS-Chem) due to differences in model structures and computational cost. The modeled ratio of surface N_r concentration to the N_r column may have variability at spatial scales finer than the horizontal resolution of global ACTMs. The impact of such scale effect (at different spatial scales) on estimated surface N_r concentration should be further studied.

Third, the satellite observation can only obtain reliable NO_2 and NH_3 column presently, and there are no available high-resolution and reliable direct HNO_3, NO_3^-, NH_4^+ retrievals. For HNO_3, NO_3^-, NH_4^+ concentrations, the satellite-based methods often applied the satellite-derived NO_2 and NH_3 concentration and the relationship

between N_r species from an ACTM (or ground-based measurements) to estimate surface HNO_3, NO_3^-, NH_4^+ concentration. With the development of satellite technology, more and more N_r species can be detected, such as HNO_3. However, at present, satellite HNO_3 products are not mature, and the spatial resolution is low. Direct, high-resolution and reliable satellite monitoring of more N_r species is critical to further developing the use of using atmospheric remote sensing to estimate N_r deposition at global and regional scales.

Fourth, estimating wet N_r deposition using satellite NO_2 and NH_3 column remains relatively uncommon. Further studies should focus on how to combine the high-resolution satellite NO_2 and NH_3 column and the ground-based monitoring data to build wet N_r deposition models to estimate wet N_r deposition at higher spatiotemporal resolution. The proposed scheme to estimate the wet N_r deposition in **Sect. 3** is statistical. As far as we know, previous studies using satellite NO_2 and NH_3 column to estimate wet N_r deposition were through a statistical way, and no studies were done from a mechanism perspective. The wet N_r deposition includes the scavenging processes of in-cloud, under-cloud and precipitation. Processed-level knowledge and models can benefit the estimation of wet N_r deposition using satellite NO_2 and NH_3 column.

7. Conclusion

The recent advances of satellite-based methods for estimating surface N_r concentration and deposition have been reviewed. Previous studies have focused on using satellite NO_2 column to estimate surface NO_2 concentrations and dry NO_2 deposition both regionally and globally. The research on calculating surface NH_3 concentration and reduced N_r deposition by satellite NH_3 data is just beginning, and some scholars have carried out estimating surface NH_3 concentration and dry NH_3

deposition on different spatial and temporal scales, but the research degree is still relatively low. We present a framework of using satellite NO_2 and NH_3 column to estimate N_r deposition based on recent advances. The proposed framework of using Gaussian function to model vertical NO_2 and NH_3 profiles can be used to convert the satellite NO_2 and NH_3 column to surface NO_2 and NH_3 concentration at any height simply and quickly. The proposed framework of using satellite NO_2 and NH_3 column to estimate wet N_r deposition is a statistical way, and further studies should be done from a mechanism perspective. Finally, we summarized current challenges of using satellite NO_2 and NH_3 column to estimate surface N_r concentration and deposition including a lack of considering NH_3 bidirectional air-surface exchanges and the problem of different spatial scales between an ACTM and satellite observation.

Acknowledgments

This study is supported by the National Natural Science Foundation of China (No. 41471343, 41425007 and 41101315) and the Chinese National Programs on Heavy Air Pollution Mechanisms and Enhanced Prevention Measures (Project No. 8 in the 2nd Special Program).

Author contributions. LL designed this study. LL, YYY and WX conducted the data analysis. All co-authors contributed to the revision of the paper.

Data availability. OMI NO_2 datasets are available at http://www.temis.nl/airpollution/no2.html. IASI NH_3 datasets are available at https://cds-espri.ipsl.upmc.fr/etherTypo/index.php?id=1700&L=1. Surface NO_2 concentration during 2005-2007 obtained by Nowlan et al. (Nowlan et al., 2014) and longterm estimates (1996-2012) by Geddes et al. (Geddes et al., 2016) are available at http://fizz.phys.dal.ca/~atmos/martin/?page_id=232. Total oxidized N_r deposition simulated by GEOS-Chem constrained with GOME, SCIAMACHY, and GOME-2

NO_2 retrievals during 1996-2014 (Geddes and Martin, 2017) is available at http://fizz.phys.dal.ca/~atmos/martin/?page_id=1520. A database of atmospheric N_r concentration and deposition from the nationwide monitoring network in China is available at https://www.nature.com/articles/s41597-019-0061-2. Measured N_r concentration and deposition datasets in the United States are available on the website: https://www.epa.gov/outdoor-air-quality-data. Measured surface NO_2 and NH_3 concentration datasets in Europe are available at https://www.nilu.no/projects/ccc/emepdata.html. Global surface NO_2 and NH_3 concentration data used to calculate the longterm trends in **Fig. 13** and **Fig. 14** have been released on the website: https://zenodo.org/record/3546517#.Xj6I4GgzY2w.

Competing interests. The authors declare no competing financial interests.

Reference

Amos, H. M., Jacob, D. J., Holmes, C. D., Fisher, J. A., Wang, Q., Yantosca, R. M., Corbitt, E. S., Galarneau, E., Rutter, A. P., and Gustin, M. S.: Gas-particle partitioning of atmospheric Hg(II) and its effect on global mercury deposition, Atmos. Chem. Phys., 11, 29441-29477, 2012.

Beer, R., Shephard, M. W., Kulawik, S. S., Clough, S. A., Eldering, A., Bowman, K. W., Sander, S. P., Fisher, B. M., Payne, V. H., Luo, M., Osterman, G. B., and Worden, J. R.: First satellite observations of lower tropospheric ammonia and methanol, Geophys. Res Lett., 35, 1-5, 10.1029/2008GL033642, 2008.

Bobbink, R., Hicks, K., Galloway, J., Spranger, T., Alkemade, R., Ashmore, M., Bustamante, M., Cinderby, S., Davidson, E., Dentener, F., Emmett, B., Erisman, J.-W., Fenn, M., Gilliam, F., Nordin, A., Pardo, L., and De Vries, W.: Global assessment of nitrogen deposition effects on terrestrial plant diversity: a synthesis, Ecological

781 Applications, 20, 30-59, doi:10.1890/08-1140.1, 2010.
782 Boersma, K. F., Eskes, H. J., Dirksen, R. J., van der A, R. J., Veefkind, J. P., Stammes,
783 P., Huijnen, V., Kleipool, Q. L., Sneep, M., Claas, J., Leitão, J., Richter, A., Zhou, Y.,
784 and Brunner, D.: An improved tropospheric NO_2 column retrieval algorithm for the
785 Ozone Monitoring Instrument, Atmospheric Measurement Techniques, 4, 1905-1928,
786 10.5194/amt-4-1905-2011, 2011.
787 Canfield, D. E., Glazer, A. N., and Falkowski, P. G.: The evolution and future of
788 Earth's nitrogen cycle, Science, 330, 192-196, 2010.
789 Cao, G. L., Zhang, X. Y., and Gong, S. L.: Emission inventories of primary particles
790 and pollutant gases for China, Science Bulletin, 56, 781-788, 2011.
791 Cheng, M., Jiang, H., Guo, Z., Zhang, X., and Lu, X.: Estimating NO_2 dry deposition
792 using satellite data in eastern China, Int. J. Remote Sens., 34, 2548-2565, 2013.
793 Coheur, P.-F., Clarisse, L., Turquety, S., Hurtmans, D., and Clerbaux, C.: IASI
794 measurements of reactive trace species in biomass burning plumes, Atmos. Chem.
795 Phys., 9, 5655-5667, 2009.
796 Crippa, M., Guizzardi, D., Muntean, M., Schaaf, E., Dentener, F., van Aardenne, J. A.,
797 Monni, S., Doering, U., Olivier, J. G. J., Pagliari, V., and Janssens-Maenhout, G.:
798 Gridded emissions of air pollutants for the period 1970–2012 within EDGAR v4.3.2,
799 Earth Syst. Sci. Data, 10, 1987-2013, 10.5194/essd-10-1987-2018, 2018.
800 Dammers, E., Palm, M., Van Damme, M., Vigouroux, C., Smale, D., Conway, S.,
801 Toon, G. C., Jones, N., Nussbaumer, E., Warneke, T., Petri, C., Clarisse, L., Clerbaux,
802 C., Hermans, C., Lutsch, E., Strong, K., Hannigan, J. W., Nakajima, H., Morino, I.,

803 Herrera, B., Stremme, W., Grutter, M., Schaap, M., Wichink Kruit, R. J., Notholt, J.,
804 Coheur, P. F., and Erisman, J. W.: An evaluation of IASI-NH_3 with ground-based
805 Fourier transform infrared spectroscopy measurements, Atmos. Chem. Phys., 16,
806 10351-10368, 10.5194/acp-16-10351-2016, 2016.
807 David, F., M, C., U, S., MA, S., JN, C., S, R., LJ, S., A, J., B, G., and JN, G.: The
808 global nitrogen cycle in the twenty-first century, Philosophical Transactions of the
809 Royal Society of London, 368, 20130164, 2013.
810 Emmons, L., Walters, S., Hess, P., Lamarque, J.-F., Pfister, G., Fillmore, D., Granier,
811 C., Guenther, A., Kinnison, D., and Laepple, T.: Description and evaluation of the
812 Model for Ozone and Related chemical Tracers, version 4 (MOZART-4),
813 Geoscientific Model Development, 3, 43-67, 2010.
814 Erisman, J. W., Sutton, M. A., Galloway, J., Klimont, Z., and Winiwarter, W.: How a
815 century of ammonia synthesis changed the world, Nat. Geosci., 1, 636-639, 2008.
816 Farquhar, G. D., Firth, P. M., Wetselaar, R., and Weir, B.: On the Gaseous Exchange
817 of Ammonia between Leaves and the Environment: Determination of the Ammonia
818 Compensation Point, Plant Physiology, 66, 710-714, 10.1104/pp.66.4.710, 1980.
819 Galloway, J. N., Dentener, F. J., Capone, D. G., Boyer, E. W., Howarth, R. W.,
820 Seitzinger, S. P., Asner, G. P., Cleveland, C., Green, P., and Holland, E.: Nitrogen
821 cycles: past, present, and future, Biogeochemistry, 70, 153-226, 2004a.
822 Galloway, J. N., Dentener, F. J., Capone, D. G., Boyer, E. W., Howarth, R. W.,
823 Seitzinger, S. P., Asner, G. P., Cleveland, C. C., Green, P. A., Holland, E. A., Karl, D.
824 M., Michaels, A. F., Porter, J. H., Townsend, A. R., and Vöosmarty, C. J.: Nitrogen

825 Cycles: Past, Present, and Future, Biogeochemistry, 70, 153-226,
826 10.1007/s10533-004-0370-0, 2004b.
827 Galloway, J. N., Townsend, A. R., Erisman, J. W., Bekunda, M., Cai, Z., Freney, J. R.,
828 Martinelli, L. A., Seitzinger, S. P., and Sutton, M. A.: Transformation of the nitrogen
829 cycle: recent trends, questions, and potential solutions, Science, 320, 889-892, 2008.
830 Geddes, J. A., Martin, R. V., Boys, B. L., and van Donkelaar, A.: Long-term trends
831 worldwide in ambient NO_2 concentrations inferred from satellite observations,
832 Environmental Health Perspectives, 124, 281, 2016.
833 Geddes, J. A., and Martin, R. V.: Global deposition of total reactive nitrogen oxides
834 from 1996 to 2014 constrained with satellite observations of NO_2 columns, Atmos.
835 Chem. Phys., 17, 10071-10091, 2017.
836 Graaf, S. C. v. d., Dammers, E., Schaap, M., and Erisman, J. W.: How are NH_3 dry
837 deposition estimates affected by combining the LOTOS-EUROS model with
838 IASI-NH3 satellite observations?, Atmos. Chem. Phys., 18, 13173-13196,
839 https://doi.org/10.5194/acp-2018-133, 2018.
840 Grell, G. A., Peckham, S. E., Schmitz, R., McKeen, S. A., Frost, G., Skamarock, W.
841 C., and Eder, B.: Fully coupled “online” chemistry within the WRF model, Atmos.
842 Environ., 39, 6957-6975, 2005.
843 Hoesly, R. M., Smith, S. J., Feng, L., Klimont, Z., Janssens-Maenhout, G., Pitkanen,
844 T., Seibert, J. J., Vu, L., Andres, R. J., Bolt, R. M., Bond, T. C., Dawidowski, L.,
845 Kholod, N., Kurokawa, J. I., Li, M., Liu, L., Lu, Z., Moura, M. C. P., O'Rourke, P. R.,
846 and Zhang, Q.: Historical (1750–2014) anthropogenic emissions of reactive gases and

847 aerosols from the Community Emissions Data System (CEDS), Geosci. Model Dev.,
848 11, 369-408, 10.5194/gmd-11-369-2018, 2018.
849 Janssens, I. A., Dieleman, W., Luyssaert, S., Subke, J. A., Reichstein, M., Ceulemans,
850 R., Ciais, P., Dolman, A. J., Grace, J., Matteucci, G., Papale, D., Piao, S. L., Schulze,
851 E. D., Tang, J., and Law, B. E.: Reduction of forest soil respiration in response to
852 nitrogen deposition, Nat. Geosci., 3, 315, 10.1038/ngeo844
853 https://www.nature.com/articles/ngeo844#supplementary-information, 2010.
854 Jia, Y., Yu, G., Gao, Y., He, N., Wang, Q., Jiao, C., and Zuo, Y.: Global inorganic
855 nitrogen dry deposition inferred from ground-and space-based measurements,
856 Scientific reports, 6, 1-11, 2016.
857 Kharol, S. K., Martin, R. V., Philip, S., Boys, B., Lamsal, L. N., Jerrett, M., Brauer,
858 M., Crouse, D. L., Mclinden, C., and Burnett, R. T.: Assessment of the magnitude and
859 recent trends in satellite-derived ground-level nitrogen dioxide over North America,
860 Atmos. Environ., 118, 236-245, 2015.
861 Kharol, S. K., Shephard, M. W., McLinden, C. A., Zhang, L., Sioris, C. E., O'Brien, J.
862 M., Vet, R., Cady-Pereira, K. E., Hare, E., Siemons, J., and Krotkov, N. A.: Dry
863 Deposition of Reactive Nitrogen From Satellite Observations of Ammonia and
864 Nitrogen Dioxide Over North America, Geophys. Res Lett., 45, 1157-1166,
865 10.1002/2017GL075832, 2018.
866 Kim, T. W., Lee, K., Duce, R., and Liss, P.: Impact of atmospheric nitrogen deposition
867 on phytoplankton productivity in the South China Sea, Geophys. Res Lett., 41, 3156–
868 3162, 2014.

869 Kuik, F., Lauer, A., Churkina, G., Denier van der Gon, H. A. C., Fenner, D., Mar, K.
870 A., and Butler, T. M.: Air quality modelling in the Berlin-Brandenburg region using
871 WRF-Chem v3.7.1: sensitivity to resolution of model grid and input data,
872 Geoscientific Model Development Discussions, 9, 4339-4363, 2016.
873 Lamarque, J. F., Kiehl, J., Brasseur, G., Butler, T., Cameron‐Smith, P., Collins, W.,
874 Collins, W., Granier, C., Hauglustaine, D., and Hess, P.: Assessing future nitrogen
875 deposition and carbon cycle feedback using a multimodel approach: Analysis of
876 nitrogen deposition, Journal of Geophysical Research: Atmospheres (1984–2012), 110,
877 2005.
878 Lamsal, L. N., Martin, R. V., van Donkelaar, A., Steinbacher, M., Celarier, E. A.,
879 Bucsela, E., Dunlea, E. J., and Pinto, J. P.: Ground-level nitrogen dioxide
880 concentrations inferred from the satellite-borne Ozone Monitoring Instrument, J.
881 Geophys. Res-Atmos., 113, 1-15, 10.1029/2007JD009235, 2008.
882 Lamsal, L. N., Martin, R. V., Parrish, D. D., and Krotkov, N. A.: Scaling relationship
883 for NO_2 pollution and urban population size: a satellite perspective, Environ. Sci.
884 Technol., 47, 7855-7861, 2013.
885 Larkin, A., Geddes, J. A., Martin, R. V., Xiao, Q., Liu, Y., Marshall, J. D., Brauer, M.,
886 and Hystad, P.: Global Land Use Regression Model for Nitrogen Dioxide Air
887 Pollution, Environ. Sci. Technol., 51, 6957-6964, 2017.
888 Larssen, T., Duan, L., and Mulder, J.: Deposition and leaching of sulfur, nitrogen and
889 calcium in four forested catchments in China: implications for acidification, Environ.
890 Sci. Technol., 45, 1192-1198, 2011.

Levine, S. Z., and Schwartz, S. E.: In-cloud and below-cloud scavenging of Nitric acid vapor, Atmospheric Environment (1967), 16, 1725-1734, https://doi.org/10.1016/0004-6981(82)90266-9, 1982.

Li, Y., Thompson, T. M., Damme, M. V., Chen, X., Benedict, K. B., Shao, Y., Day, D., Boris, A., Sullivan, A. P., and Ham, J.: Temporal and Spatial Variability of Ammonia in Urban and Agricultural Regions of Northern Colorado, United States, Atmos. Chem. Phys., 17, 1-50, 2017.

Liu, H., Jacob, D. J., Bey, I., and Yantosca, R. M.: Constraints from 210Pb and 7Be on wet deposition and transport in a global three-dimensional chemical tracer model driven by assimilated meteorological fields, J. Geophys. Res-Atmos., 106, 12109-12128, 10.1029/2000JD900839, 2001.

Liu, L., Zhang, X., Xu, W., Liu, X., Lu, X., Chen, D., Zhang, X., Wang, S., and Zhang, W.: Estimation of monthly bulk nitrate deposition in China based on satellite NO_2 measurement by the Ozone Monitoring Instrument, Remote Sens. Environ., 199, 93-106, 2017a.

Liu, L., Zhang, X., Xu, W., Liu, X., Lu, X., Wang, S., Zhang, W., and Zhao, L.: Ground Ammonia Concentrations over China Derived from Satellite and Atmospheric Transport Modeling, Remote Sens., 9, 467, 2017b.

Liu, L., Zhang, X., Zhang, Y., Xu, W., Liu, X., Zhang, X., Feng, J., Chen, X., Zhang, Y., Lu, X., Wang, S., Zhang, W., and Zhao, L.: Dry Particulate Nitrate Deposition in China, Environ. Sci. Technol., 51, 5572-5581, 10.1021/acs.est.7b00898, 2017c.

Liu, L., Zhang, X., Wong, A. Y. H., Xu, W., Liu, X., Li, Y., Mi, H., Lu, X., Zhao, L.,

913 Wang, Z., and Wu, X.: Estimating global surface ammonia concentrations inferred
914 from satellite retrievals, Atmos. Chem. Phys., 19, 12051-12066,
915 10.5194/acp-2019-184, 2019.
916 Liu, L., Zhang, X., Xu, W., Liu, X., Wei, J., Wang, Z., and Yang, Y.: Global estimates
917 of dry ammonia deposition inferred from space-measurements, Sci.Total Environ.,
918 730, 139189, https://doi.org/10.1016/j.scitotenv.2020.139189, 2020.
919 Liu, X., Duan, L., Mo, J., Du, E., Shen, J., Lu, X., Zhang, Y., Zhou, X., He, C., and
920 Zhang, F.: Nitrogen deposition and its ecological impact in China: An overview,
921 Environ. Pollut., 159, 2251-2264, http://dx.doi.org/10.1016/j.envpol.2010.08.002,
922 2011.
923 Liu, X., Xu, W., Duan, L., Du, E., Pan, Y., Lu, X., Zhang, L., Wu, Z., Wang, X.,
924 Zhang, Y., Shen, J., Song, L., Feng, Z., Liu, X., Song, W., Tang, A., Zhang, Y., Zhang,
925 X., and Collett, J. L.: Atmospheric Nitrogen Emission, Deposition, and Air Quality
926 Impacts in China: an Overview, Curr. Pollut. Rep., 3, 65-77,
927 10.1007/s40726-017-0053-9, 2017d.
928 Lu, X., Jiang, H., Zhang, X., Liu, J., Zhang, Z., Jin, J., Wang, Y., Xu, J., and Cheng,
929 M.: Estimated global nitrogen deposition using NO_2 column density, Int. J. Remote
930 Sens., 34, 8893-8906, 2013.
931 Mari, C., Jacob, D. J., and Bechtold, P.: Transport and scavenging of soluble gases in
932 a deep convective cloud, J. Geophys. Res-Atmos., 105, 22255-22268, 2000.
933 Nadelhoffer, K. J., Emmett, B. A., Gundersen, P., Kjønaas, O. J., Koopmans, C. J.,
934 Schleppi, P., Tietema, A., and Wright, R. F.: Nitrogen deposition makes a minor

935 contribution to carbon sequestration in temperate forests, Nature, 398, 145,
936 10.1038/18205, 1999.
937 Nemitz, E., Flynn, M., Williams, P. I., Milford, C., Theobald, M. R., Blatter, A.,
938 Gallagher, M. W., and Sutton, M. A.: A Relaxed Eddy Accumulation System for the
939 Automated Measurement of Atmospheric Ammonia Fluxes, Water, Air and Soil
940 Pollution: Focus, 1, 189-202, 10.1023/A:1013103122226, 2001.
941 Nicolas, G., and Galloway, J. N.: An Earth-system perspective of the global nitrogen
942 cycle, Nature, 451, 293-296, 2008.
943 Nowlan, C., Martin, R., Philip, S., Lamsal, L., Krotkov, N., Marais, E., Wang, S., and
944 Zhang, Q.: Global dry deposition of nitrogen dioxide and sulfur dioxide inferred from
945 space-based measurements, Global Biogeochem. Cy., 28, 1025-1043, 2014.
946 Paerl, H. W., Gardner, W. S., Mccarthy, M. J., Peierls, B. L., and Wilhelm, S. W.:
947 Algal blooms: noteworthy nitrogen, Science, 346, 175, 2014.
948 Pan, Y., Wang, Y., Tang, G., and Wu, D.: Wet and dry deposition of atmospheric
949 nitrogen at ten sites in Northern China, Atmos. Chem. Phys., 12, 6515-6535, 2012.
950 Ronsmans, G., Langerock, B., Wespes, C., Hannigan, J. W., Hase, F., Kerzenmacher,
951 T., Mahieu, E., Schneider, M., Smale, D., Hurtmans, D., De Mazière, M., Clerbaux, C.,
952 and Coheur, P. F.: First characterization and validation of FORLI-HNO3 vertical
953 profiles retrieved from IASI/Metop, Atmos. Meas. Tech., 9, 4783-4801,
954 10.5194/amt-9-4783-2016, 2016.
955 Schrader, F., Brümmer, C., Flechard, C. R., Wichink Kruit, R. J., van Zanten, M. C.,
956 Zöll, U., Hensen, A., and Erisman, J. W.: Non-stomatal exchange in ammonia dry

957 deposition models: comparison of two state-of-the-art approaches, Atmos. Chem.
958 Phys., 16, 13417-13430, 10.5194/acp-16-13417-2016, 2016.
959 Shen, J., Li, Y., Liu, X., Luo, X., Tang, H., Zhang, Y., and Wu, J.: Atmospheric dry
960 and wet nitrogen deposition on three contrasting land use types of an agricultural
961 catchment in subtropical central China, Atmos. Environ., 67, 415-424,
962 http://dx.doi.org/10.1016/j.atmosenv.2012.10.068, 2013.
963 Stevens, C. J., Dise, N. B., Mountford, J. O., and Gowing, D. J.: Impact of Nitrogen
964 Deposition on the Species Richness of Grasslands, Science, 303, 1876-1879,
965 10.1126/science.1094678, 2004.
966 Sutton, M. A., Tang, Y. S., Miners, B., and Fowler, D.: A New Diffusion Denuder
967 System for Long-Term, Regional Monitoring of Atmospheric Ammonia and
968 Ammonium, Water Air & Soil Pollution Focus, 1, 145-156, 2001.
969 Sutton, M. A., Bleeker, A., Howard, C. M., Bekunda, M., Grizzetti, B., Vries, W. D.,
970 Grinsven, H. J. M. V., Abrol, Y. P., Adhya, T. K., and Billen, G.: Our Nutrient World:
971 the challenge to produce more food and energy with less pollution, 2013.
972 Tan, J., Fu, J. S., Dentener, F., Sun, J., Emmons, L., Tilmes, S., Sudo, K., Flemming,
973 J., Jonson, J. E., and Gravel, S.: Multi-model study of HTAP II on sulfur and nitrogen
974 deposition, Atmos. Chem. Phys., 18, 1-36, 2018.
975 Van Damme, M., Clarisse, L., Dammers, E., Liu, X., Nowak, J., Clerbaux, C.,
976 Flechard, C., Galy-Lacaux, C., Xu, W., and Neuman, J.: Towards validation of
977 ammonia (NH_3) measurements from the IASI satellite, Atmospheric Measurement
978 Techniques, 7, 12125-12172, 2014a.

979 Van Damme, M., Wichink Kruit, R., Schaap, M., Clarisse, L., Clerbaux, C., Coheur, P.
980 F., Dammers, E., Dolman, A., and Erisman, J.: Evaluating 4 years of atmospheric
981 ammonia (NH_3) over Europe using IASI satellite observations and LOTOS-EUROS
982 model results, J. Geophys. Res-Atmos., 119, 9549-9566, 2014b.
983 Van der Graaf, S. C., Dammers, E., Schaap, M., and Erisman, J. W.: Technical note:
984 How are NH_3 dry deposition estimates affected by combining the LOTOS-EUROS
985 model with IASI-NH_3 satellite observations?, Atmos. Chem. Phys., 18, 13173-13196,
986 10.5194/acp-18-13173-2018, 2018.
987 Vet, R., Artz, R. S., Carou, S., Shaw, M., Ro, C.-U., Aas, W., Baker, A., Bowersox, V.
988 C., Dentener, F., Galy-Lacaux, C., Hou, A., Pienaar, J. J., Gillett, R., Forti, M. C.,
989 Gromov, S., Hara, H., Khodzher, T., Mahowald, N. M., Nickovic, S., Rao, P. S. P., and
990 Reid, N. W.: A global assessment of precipitation chemistry and deposition of sulfur,
991 nitrogen, sea salt, base cations, organic acids, acidity and pH, and phosphorus, Atmos.
992 Environ., 93, 3-100, http://dx.doi.org/10.1016/j.atmosenv.2013.10.060, 2014.
993 Vitousek, P. M., Aber, J. D., Howarth, R. W., Likens, G. E., Matson, P. A., Schindler,
994 D. W., Schlesinger, W. H., and Tilman, D. G.: Human alteration of the global nitrogen
995 cycle: sources and consequences, Ecol. Appl., 7, 737-750, 1997.
996 Wesely, M., and Hicks, B.: Some factors that affect the deposition rates of sulfur
997 dioxide and similar gases on vegetation, Journal of the Air Pollution Control
998 Association, 27, 1110-1116, 1977.
999 Whitburn, S., Van Damme, M., Clarisse, L., Bauduin, S., Heald, C. L., Hadji-Lazaro,
1000 J., Hurtmans, D., Zondlo, M. A., Clerbaux, C., and Coheur, P. F.: A flexible and robust

neural network IASI-NH_3 retrieval algorithm, J. Geophys. Res-Atmos., 121, 6581-6599, 10.1002/2016JD024828, 2016.

Williams, J. E., Boersma, K. F., Le Sager, P., and Verstraeten, W. W.: The high-resolution version of TM5-MP for optimized satellite retrievals: description and validation, Geosci. Model Dev., 10, 721-750, 10.5194/gmd-10-721-2017, 2017.

Wong, D. C., Pleim, J., Mathur, R., Binkowski, F., Otte, T., Gilliam, R., Pouliot, G., Xiu, A., Young, J. O., and Kang, D.: WRF-CMAQ two-way coupled system with aerosol feedback: software development and preliminary results, Geosci. Model Dev., 5, 299-312, 10.5194/gmd-5-299-2012, 2012.

Xu, W., Luo, X. S., Pan, Y. P., Zhang, L., Tang, A. H., Shen, J. L., Zhang, Y., Li, K. H., Wu, Q. H., Yang, D. W., Zhang, Y. Y., Xue, J., Li, W. Q., Li, Q. Q., Tang, L., Lv, S. H., Liang, T., Tong, Y. A., Liu, P., Zhang, Q., Xiong, Z. Q., Shi, X. J., Wu, L. H., Shi, W. Q., Tian, K., Zhong, X. H., Shi, K., Tang, Q. Y., Zhang, L. J., Huang, J. L., He, C. E., Kuang, F. H., Zhu, B., Liu, H., Jin, X., Xin, Y. J., SHi, X. K., Du, E. Z., Dore, A. J., Tang, S., Collett Jr, J. L., Goulding, K., Sun, Y. X., Ren, J., Zhang, F. S., and Liu, X. J.: Quantifying atmospheric nitrogen deposition through a nationwide monitoring network across China, Atmos. Chem. Phys., 15, 12345-12360, 2015.

Yu, G., Jia, Y., He, N., Zhu, J., Chen, Z., Wang, Q., Piao, S., Liu, X., He, H., Guo, X., Wen, Z., Li, P., Ding, G., and Goulding, K.: Stabilization of atmospheric nitrogen deposition in China over the past decade, Nat. Geosci., 12, 424-429, 10.1038/s41561-019-0352-4, 2019.

Zhang, L., Wright, L. P., and Asman, W. A. H.: Bi-directional air-surface exchange of

1023 atmospheric ammonia: A review of measurements and a development of a big-leaf
1024 model for applications in regional-scale air-quality models, J. Geophys. Res-Atmos.,
1025 115, 898-907, 2010.
1026 Zhang, L., Jacob, D. J., Knipping, E. M., Kumar, N., Munger, J. W., Carouge, C., Van
1027 Donkelaar, A., Wang, Y., and Chen, D.: Nitrogen deposition to the United States:
1028 distribution, sources, and processes, Atmos. Chem. Phys., 12 4539-4554, 2012.
1029 Zhang, Q., Streets, D. G., Carmichael, G. R., He, K., Huo, H., Kannari, A., Klimont,
1030 Z., Park, I., Reddy, S., and Fu, J.: Asian emissions in 2006 for the NASA INTEX-B
1031 mission, Atmos. Chem. Phys., 9, 5131-5153, 2009.
1032 Zhang, X. Y., Lu, X. H., Liu, L., Chen, D. M., Zhang, X. M., Liu, X. J., and Zhang, Y.:
1033 Dry deposition of NO_2 over China inferred from OMI columnar NO_2 and atmospheric
1034 chemistry transport model, Atmos. Environ., 169, 2017.
1035 Zhang, X. Y., Chuai, X. W., Liu, L., Zhang, W. T., Lu, X. H., Zhao, L. M., and Chen,
1036 D. M.: Decadal Trends in Wet Sulfur Deposition in China Estimated From OMI SO_2
1037 Columns, J. Geophys. Res-Atmos., 123, 10796-10811, 10.1029/2018JD028770, 2018.
1038 Zhao, X., Chen, L., and Zhang, H.: Nitrate and ammonia contaminations in drinking
1039 water and the affecting factors in Hailun, northeast China, Journal of Environmental
1040 Health, 75, 28, 2013.
1041 Zhao, Y., Zhang, L., Chen, Y., Liu, X., Xu, W., Pan, Y., and Duan, L.: Atmospheric
1042 nitrogen deposition to China: A model analysis on nitrogen budget and critical load
1043 exceedance, Atmos. Environ., 153, 32-40,
1044 http://dx.doi.org/10.1016/j.atmosenv.2017.01.018, 2017.

1045